

Optical and electrical properties of Ta-doped ZnSnO₃ transparent conducting films by sol–gel

Siqi Cai¹ · Yiming Li¹ · Xiao Chen¹ · Yuanyuan Ma¹ · Xiaojun Liu¹ · Yunqiu He^{1,2}

Received: 15 November 2015 / Accepted: 15 February 2016 / Published online: 4 April 2016
© Springer Science+Business Media New York 2016

Abstract Undoped and Ta-doped ZnSnO₃ thin films with different Ta concentrations were deposited on glass substrates by using sol–gel spin coating method. Effects of Ta concentration (0–4 at.%) on structure, surface morphology, electrical and optical properties were investigated. Single phase and crystallinity deterioration were observed in the XRD spectrum. The porosity rate was calculated by processed SEM figures with different dopant content. XPS spectrum and results of Hall measurement indicated that there might be substitution of Ta⁵⁺ for Sn⁴⁺ dominantly when doping content is lower than 2 at.% and main substitution of Ta⁵⁺ for Zn²⁺ when doping content is up to 2 at.%. A minimum resistivity of 1.716 Ω cm were obtained for films with 2 at.% Ta. The optical transmittances clearly exhibited absorption edges shift to longer wavelength, and those in the visible range increased up to over 91 % with increasing Ta concentration. The work function of undoped and 2 at.% ZnSnO₃ are 5.17 and 5.06 eV respectively, which are higher than ITO, FTO.

1 Introduction

Demands for transparent conducting oxides (TCO) are rapidly increasing in technological applications of optoelectronic devices such as solar cells, liquid crystal

displays, organic photovoltaics, light emitting diode (LED), and organic light-emitting diodes (OLEDs) etc. [1–4]. ITO is most widely used TCO in above applications for its excellent conductivity, good optical properties and the ease of acid etching. However, the high price of indium has endangered the large scale use of ITO. Meanwhile, ITO is also limited to meet the forthcoming requirement in today's flat-panel industry due to the lower work function. For example, OLED host materials' highest occupied molecular orbital (HOMO) is typically ~6 eV, which is much too deep to inject charge from these TCOs whose typical work function is 4.4–4.8 eV [5]. So that, searching TCOs with both good electric and optical property and higher work function is becoming more and more relevant. The effort to improve the conductivity without decreasing the transparency was done by synthesizing phase-segregated multiple TCOs [6]. In the research of Northwestern University [7], the band gap, carrier concentration and work function could be modified by varying the composition of ternary TCOs. So that much attention has been attracted to ternary systems which could be designed as new materials with improved optical and electrical properties especially work function [1]. Ternary systems composed of heavy metal cations with $(n - 1)d^{10}ns^0$ ($n \geq 4$) electronic configurations constitute attractive compounds, among which, Cd–Sn–O, In–Zn–O (IZO), In–Ga–Zn–O (IGZO), and Zn–Sn–O (ZTO) are most popular for their lower cost and good thermal stabilities [8–11].

Zn–Sn–O is n-type semiconductor with a wide direct optical band gap of 3.35–3.89 eV [10] and a comparable conductivity to ITO [12], which makes it an attractive TCO material. Perovskite ZnSnO₃ and spinel Zn₂SnO₄ are two crystalline phases of ZTO which could be fabricated by different synthetic methods [13–18]. And ZnSnO₃ was predicted to have better conductivity and higher work

✉ Yunqiu He
heyunqiu@tongji.edu.cn

¹ School of Material Science and Engineering, Tongji University, Shanghai 200092, People's Republic of China

² Key Laboratory of Advanced Civil Engineering Materials of Ministry of Education, Tongji University, Shanghai 200092, People's Republic of China

function than Zn_2SnO_4 [17, 19]. The reported work function of ZnSnO_3 is 5.3 eV that is much higher than ITO (4.7 eV) [20, 21]. In addition, ZnSnO_3 has higher transparency and more stable than ITO and FTO [15]. These advantages make ZnSnO_3 with great application potential as TCOs.

ZnSnO_3 films were commonly fabricated by sputtering. However, ZnO , SnO_2 , Zn_2SnO_4 coexist with ZnSnO_3 , which makes it complex to analyze the properties of ZnSnO_3 . In our previous works [22], pure ZnSnO_3 thin films were fabricated by sol–gel and more interstitial Zn^{2+} were found beneficial for conductivity. To improve the conductivity of ZnSnO_3 thin films, tantalum is doped into ZnSnO_3 for its high valence, suitable ionic radius, ease of handling, low material toxicity and low cost [23–26]. In this study, transparent and conductive Ta-doped ZnSnO_3 thin films were fabricated by sol–gel method with different doping levels of Ta. The effects of Ta on the structure, morphological, chemical station of ions, electrical and optical properties of films were investigated. Work functions were also tested for a comparison with common TCOs.

2 Experimental

All chemicals were of analytical grade and were used as received without further purification. Zinc acetate dihydrate ($\text{Zn}(\text{Ac})_2 \cdot 2\text{H}_2\text{O}$) and tin chloride pentahydrate ($\text{SnCl}_4 \cdot 5\text{H}_2\text{O}$) were served as raw materials for ZnSnO_3 , tantalum pentachloride (TaCl_5) acted as doping source.

In this study, the concentration of cation ($[\text{Ta}] + [\text{Zn}] + [\text{Sn}]$) was fixed at 0.4 mol/L, the molar ratio of Ta content was varied from 0.5 to 4 %. In a typical procedure, Zinc acetate dihydrate was dissolved in 30 ml 2-methoxyethanol ($\text{HOCH}_2\text{CH}_2\text{OCH}_3$), and then a stabilizer of monoethanolamine (MEA) was added to the blended solution to prevent precipitation and the molar ratio of MEA to cation was maintained at 0.9. After that, $\text{SnCl}_4 \cdot 5\text{H}_2\text{O}$ was added to Zinc acetate solution with the ratio of Zn to Sn at 1:1, and a ZnSnO_3 precursor was produced after a while.

The Ta-doped ZnSnO_3 precursor solution were prepared by combining 52 ml anhydrous ethanol with TaCl_5 dissolved into ZnSnO_3 precursor solution as prepared above under stirring for 15 min at room temperature. The Ta-doped ZnSnO_3 precursor solution was stirred at 80 °C for 4 h with a reflux condensation to yield a clear and transparent sol. The sol aged for 24 h before the deposition.

All Ta-doped ZnSnO_3 sol–gel films were spin coated onto pre-cleaned quartz glass substrates with a size of 30 mm × 30 mm × 1 mm at a rotation speed of 3000 rpm for 20 s. Each as-coated film was heated at 300 °C for

10 min to evaporate the solvent, water, and partial organics. After the spin coating and drying procedures were repeated three times, these dried sol–gel films were thermally annealed from room temperature to 1000 °C at a heating rate of 2 °C/min and then maintained at 1000 °C for 6 h under air ambiance to achieve crystalline Ta-doped ZnSnO_3 thin films.

The annealing ZnSnO_3 :Ta thin films were characterized further for their structural, morphological, electrical, chemical, optical properties and work function. The phase and crystallinity of the films were determined by X-ray diffraction (XRD: D/max-rB 24 kW, $V = 40$ kV, $I = 60$ mA, Cu Ka, $\lambda = 0.15418$ nm). The surface morphology was taken with a field emission scanning electron microscope (FE-SEM, Hitachi S-4800, 3 kV). The chemical composition was determined by X-ray photoelectron spectroscopy (XPS, Thermo ESCALAB 250Xi). The detailed XPS spectra were recorded after sputtering with Ar^+ ions (500 eV, 30 s) to remove the surface contamination of films. In the work of Kim et al. [27], a low energy (100–1000 eV) Ar^+ sputtering is considered helpful to clean a dirty surface. All oxides with $-\Delta G_f^0$ above 118 kcal/mol were stable when exposed to Ar^+ ions while those with $-\Delta G_f^0$ below 60 kcal/mol were reduced. The $-\Delta G_f^0$ of ZnO , SnO_2 , Ta_2O_5 were 76, 124, 471 kcal/mol respectively, which means the Ar^+ ions (below 1000 eV) can be used to clean the surface without reducing Ta, Sn^{4+} , Zn^{2+} [28]. The electrical conductivity, carrier concentration and Hall mobility of these films were measured at room temperature by Accent HL5500 Hall System in vander Pauw configuration. The four contact electrodes were gold in each sample. Optical transmittance spectra of these films were investigated with a UV–Vis spectrophotometer (UV 22501PC).

Work function of films were characterized by electrochemical impedance technique with electrochemical workstation (CHI660C). A transfer techniques was used to prepare tested samples: 5 wt% PMMA dissolved in acetone, then the solution was spin-coated (1000 r/min 30 s) on the top of the ZnSnO_3 and Ta doped films deposited on silica glass. After the samples were heated for 30 min at 70 °C, they were dipped in dilute hydrofluoric acid solution (deionized water: HF = 1:1 and drops of ethanol to reduce surface tension) for 2 h. Then, the films were transferred to FTO substrate. After the transfer process, these transferred films were heated from room temperature to 400 °C at a heating rate of 2 °C/min and then maintained at 400 °C for 1 h under air ambiance to remove PMMA foils. Then, the samples for test were prepared. Mott–Schottky curves were tested in a three-electrode cell to acquire work function. Platinum foil was used as counter electrode and a Ag/Ag^+ electrode as the reference electrode in which the

electrolytes was anhydrous acetonitrile with 0.01 M/ AgNO₃ dissolved. The samples prepared as above were used as working electrode. Electrolytes in cell was deoxygenized acetonitrile dissolved with 0.01 M/ LiClO₄, and the test frequency was 100 Hz.

3 Results and discussion

3.1 XRD analysis of films

Figure 1 shows XRD spectrum of Ta-doped ZnSnO₃ films with 0.5 and 4 at.% Ta contents. Both films are in single phase without any secondary phases. The result indicates that Ta is incorporated into ZnSnO₃. 2θ positions of each peak match well with ZnSnO₃ (JCPDS No. 28-1486). When Ta was incorporated, the intensities of the strong diffraction peaks decrease significantly. This might be due to Ta doping in the ZnSnO₃ lattice, and deteriorating the crystallinity of the ZnSnO₃ thin films.

3.2 Morphological analysis of films

Figure 2 shows SEM images of the ZnSnO₃:Ta thin films with different Ta concentrations: (a) 0, (b) 0.5, (c) 2 and (d) 4 at.%. All thin films exhibited nanoparticles and particle-like pore structures. The particle-like pore structures were particularly apparent in the sol–gel synthesized thin films [29]. It is obvious that the grain size decreases with the Ta concentration increasing from undoped to 4 at.%. This result is in accord with the crystallinity deterioration observed in the XRD graphs. In processed SEM images, the porosity rate was calculated by Image-Pro Plus by

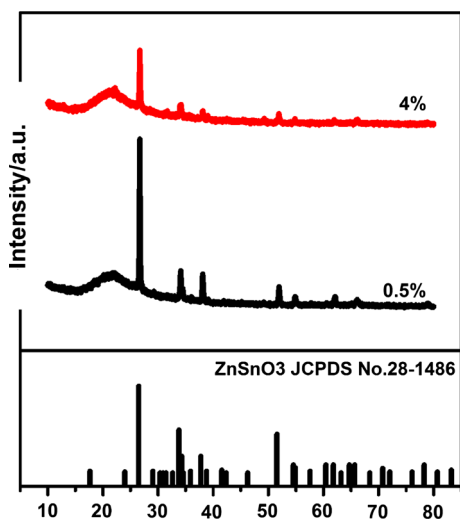


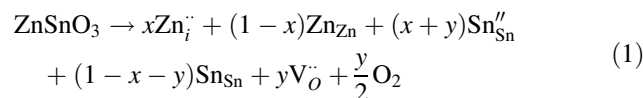
Fig. 1 XRD patterns of ZnSnO₃:Ta thin films with different Ta concentrations

calculating the pores area (red region) and nanoparticles area (blue region) ratio in the SEM photos. And the porosity rate of thin films with different Ta concentrations: 0, 0.5, 2 and 4 at.% are 34, 35, 34 and 34 %, respectively. The result indicates that though the pores' shape change which is due to the decrease of grain size in films with increasing tantalum concentration, the porosity in the films is nearly the same.

3.3 X-ray photoelectron spectroscopy analysis

The chemical binding states were taken by X-ray photoelectron spectroscopy (XPS). The detailed XPS spectra of Ta4f, O1s, Sn3d and Zn2p in films with different Ta concentrations are recorded. XPS spectra for Ta4f of ZnSnO₃:Ta thin films with different Ta concentrations are shown in Fig. 3. And these films have the same binding energies of Ta4f7/2(26.20 eV) and Ta4f5/2(28.03 eV), which is well accorded to the binding energy of Ta⁵⁺ [27, 28, 30, 31]. Thus, all the Ta contents in the films are in a chemical state of Ta⁵⁺ without other states.

Figure 4 shows the fitted O1s XPS spectrum of the Ta-doped ZnSnO₃ films with different molar concentrates: (a) 0, (b) 0.5, (c) 1, (d) 2 and (e) 4 at.%. The O1s peaks are decomposed into three components, of which appears at 529.60 ± 0.3 eV (O_I, normally defined as oxygen adjacent to low valence tin (O–Sn²⁺) [32] or interstitial Zn²⁺ (O–Zn_i²⁺) [22, 33]), 530.45 ± 0.3 eV (O_{II}, O²⁻ in the proper sites of ZnSnO₃ crystal lattice (Zn–O–Sn) [32, 34]) and 531.40 ± 0.3 eV (O_{III}, oxygen vacancy [14, 35]), respectively. And oxygen of free hydroxyl groups due to surface contamination [14] disappear after sputter cleaning. The details of the fitted O1s spectrum are summarized in Table 1. With the increase of Ta content, the percentage of O_I (O–Sn²⁺, O–Zn_i²⁺) is always increasing: 6.73 (0 at.%), 13.50 (0.5 at.%), 15.41 (1 at.%), 16.52 (2 at.%), 21.80 % (4 at.%). This is due to the substitution of Ta⁵⁺ in ZnSnO₃ crystal lattice. On the contrary, the area of oxygen vacancy is on the decline: 30.94 (0 %), 27.91 (0.5 %), 23.64 (1 %), 22.28 (2 %), 22.12 % (4 %). The result indicates that tantalum has significant effect on the decrease of vacancy when doping concentration is no more than 1 at.%, and the percentage of oxygen vacancy are nearly the same when the content is more than 1 at.%. The oxygen vacancy in undoped film is as high as 30.94 %, which may be produced in the process Eq. 1.



Sn²⁺ (Sn_{Sn}^{••}) in Eq. 1 is assumed to be generated by double ionization of tin at high growth temperature [32, 36]. Sn²⁺ (Sn_{Sn}^{••}) is assumed to balance the positive charge

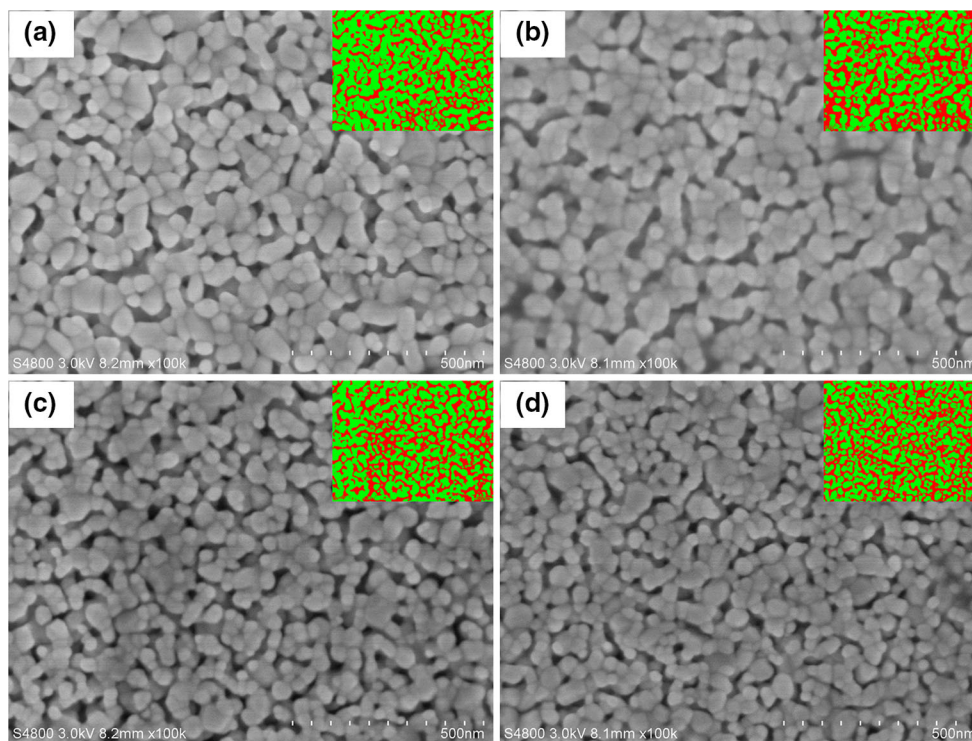


Fig. 2 SEM images and processed SEM images of ZnSnO₃:Ta thin films with different Ta concentrations: **a** 0 at.%, **b** 0.5 at.%, **c** 2 at.%, and **d** 4 at.%. The inserted pictures were processed SEM images by

Image-Pro Plus software in which the *red region* and *green region* represent pores and nanoparticles, respectively (Color figure online)

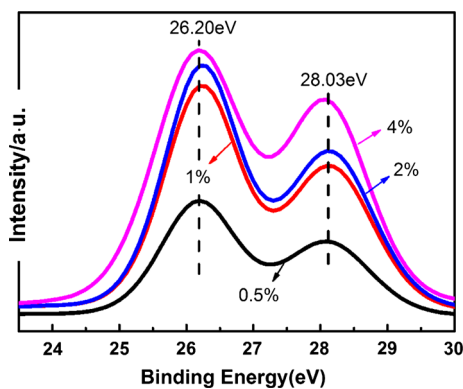


Fig. 3 XPS spectra for Ta4f of ZnSnO₃:Ta thin films with different Ta concentrations: 0.5, 1, 2, and 4 at.%

of V_{O}^{\bullet} and Zn_i^{\bullet} and other defects with positive charge. And interstitial zinc might be caused by oxygen loss, which is expected to act as a double ionized donor [37].

Figure 5 shows the fitted Sn3d XPS spectrum of the Ta-doped ZnSnO₃ films with different Ta concentrations: (a) 0, (b) 0.5, (c) 1, (d) 2 and (e) 4 at.%, and the details of the fitted Sn3d spectrum are presented in Table 2. The Sn3d peaks are decomposed into three Sn3d components, of which appear at 485.55 ± 0.3 eV (Sn_{I} , low valence tin Sn^{2+} [32, 38, 39]), 486.3 ± 0.3 eV (Sn_{II} , Sn^{4+} in ZnSnO₃

crystal lattice [32, 34]) and 487.2 ± 0.3 eV (Sn_{III} , Sn^{4+} adjacent to oxygen vacancy [14]). With the Ta content increasing, the Sn^{2+} (Sn_{I}) concentration keeps increasing to balance positive charges generated by the substitution of tantalum in ZnSnO₃ crystal lattice and a sharp amplification is observed at 2 at.% tantalum than other doping content. This behavior may lead to more oxygen adjacent to Sn_{I}^{\bullet} as shown in Table 1. Otherwise, Sn^{2+} is 14.60 % in the pure ZnSnO₃ film, which can be explained by Eq. 1. Meanwhile, Sn^{4+} adjacent to oxygen vacancy (Sn_{III}) is in decline from 21.36 (0 at.%) to 16.36 % (4 at.%), which is in good agreement with the variation tendency of oxygen vacancy in Table 1.

Figure 6 shows the fitted Zn2p XPS spectrum of the Ta-doped ZnSnO₃ films with different Ta concentrations: (a) 0, (b) 0.5, (c) 1, (d) 2 and (e) 4 at.%, and the details of the fitted Zn2p spectrum are presented in Table 3. Zn2p peaks are decomposed into three Zn2p components, of which appears at 1020.50 ± 0.3 eV (Zn_{I} , interstitial Zn^{2+} [14]), 1021.80 ± 0.3 eV (Zn_{II} , Zn^{2+} in the proper site of ZnSnO₃ crystal lattice [14]) and 1022.80 ± 0.3 eV (Zn_{III} , Zn^{2+} adjacent to oxygen vacancy [22, 33]). As the table shows, when the dopant content is below 2 %, the percentage of interstitial Zn^{2+} decreases: 9.36 (0 at.%), 8.52 (0.5 at.%), 8.44 % (1 at.%). However, when the dopant content increase to 2 at.%, the percentage of

Fig. 4 XPS spectra for O 1 s of ZnSnO₃:Ta thin films with different Ta concentrations: **a** 0 at.%, **b** 0.5 at.%, **c** 1 at.%, **d** 2 at.% and **e** 4 at.%

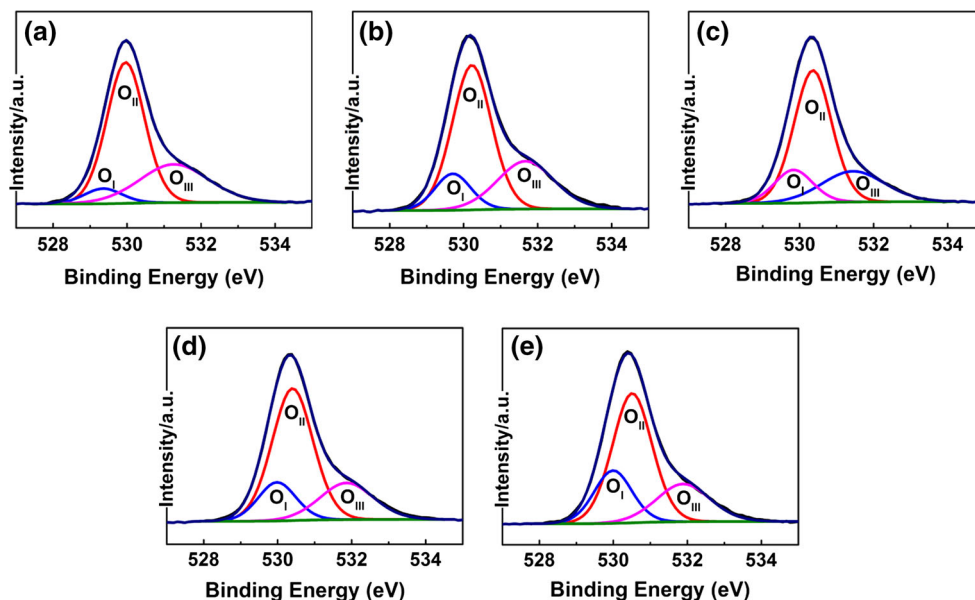
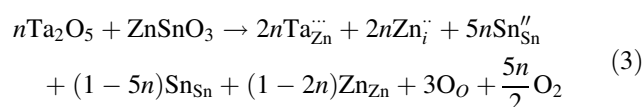
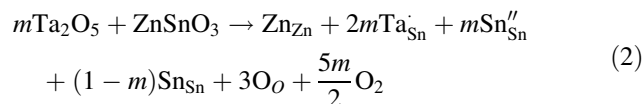


Table 1 XPS peak position of O 1 s in ZnSnO₃:Ta thin films with different Ta concentrations

Doping concentration (at.%)	O _I 1s	O _{II} 1s	O _{III} 1s
0	529.55 eV	530.16 eV	531.47 eV
	6.73 %	62.31 %	30.94 %
0.5	529.71 eV	530.22 eV	531.61 eV
	13.50 %	58.59 %	27.91 %
1	529.84 eV	530.36 eV	531.44 eV
	15.41 %	60.91 %	23.64 %
2	529.68 eV	530.10 eV	531.56 eV
	16.52 %	61.20 %	22.28 %
4	529.69 eV	530.21 eV	531.59 eV
	21.80 %	56.08 %	22.12 %

interstitial Zn²⁺ begin to increase: 10.29 (2 at.%), 10.77 % (4 at.%). This behavior might be a result of Ta⁵⁺ substitution for Zn²⁺. Otherwise, interstitial Zn²⁺ is 9.36 % in the pure ZnSnO₃ film, which can be explained by Eq. 1. At the same time, the concentration of Zn²⁺ adjacent to oxygen vacancy is in decline from 11.90 (0 at.%) to 8.60 % (4 at.%), which is in accord with the variation tendency of oxygen vacancy in Table 1.

According to previous XPS analysis of oxygen and tin as well as zinc in pure and Ta doped ZnSnO₃ films, it could be concluded that: with the increase of tantalum concentration, the Sn²⁺ increases continuously and oxygen vacancy is always in decline. However, the variation tendency of interstitial Zinc changes at 2 at.% doping content. These behaviors might be caused by different substitution mechanism of tantalum described by Eqs. 2 and 3.



Equations 2 and 3 show the mechanism of Ta⁵⁺ substitute for Sn⁴⁺ and Zn²⁺ respectively. Where, $\frac{5m}{2}\text{O}_2$ and $\frac{5n}{2}\text{O}_2$ are surplus oxygen introduced by Ta₂O₅, which might cause the reduce of oxygen vacancy as previous analysis shows. According to previous XPS analysis, the interstitial zinc decreases when the content is below 2 at.%, which might be a result of oxygen vacancy decrease. Whereas, interstitial zinc begins to increase and a larger amplification of Sn²⁺ is observed at 2 at.% tantalum content. These results indicate that Zn²⁺ is substituted dominantly by Ta⁵⁺ when Ta content is above 2 at.%, and Sn⁴⁺ is substituted dominantly when Ta content is below 2 at.%.

3.4 Electrical properties

The resistivity, carrier concentration and Hall mobility of Ta-doped ZnSnO₃ films prepared with different molar concentrations are summarized in Table 4 and the variation tendency are shown in Fig. 8. The negative sign of Hall coefficient confirms the films n-type semiconductors. Equation 4 shows the relationship among carrier concentration (*n*), charge mobility (*μ*), electronic charge (*q*) and the resistivity (*ρ*) in films:

$$\rho = \frac{1}{q n \mu} \quad (4)$$

Fig. 5 XPS spectra for Sn3d of ZnSnO₃:Ta thin films with different Ta concentrations: **a** 0 at.%, **b** 0.5 at.%, **c** 1 at.%, **d** 2 at.% and **e** 4 at.%

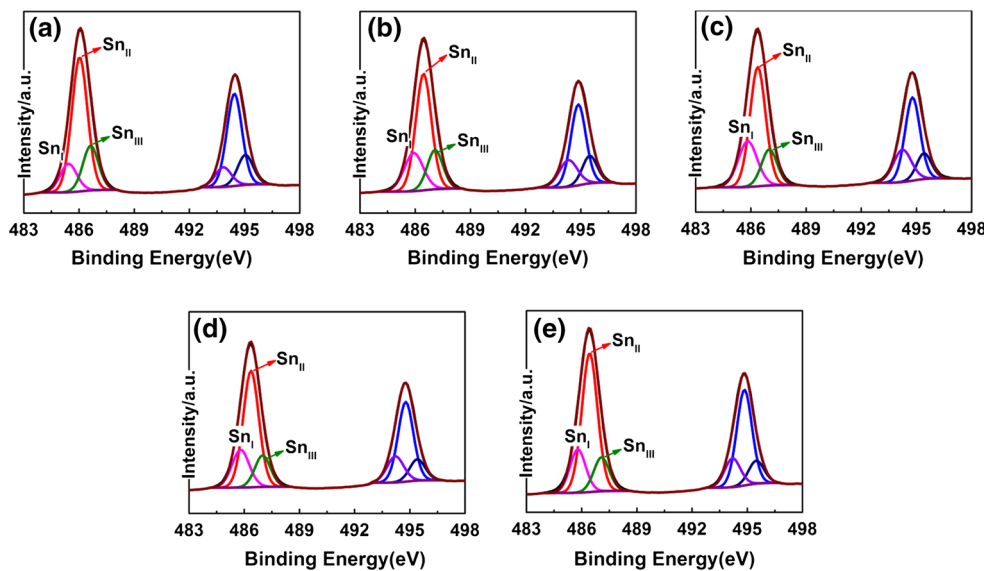


Table 2 XPS peak position of Sn 3d in ZnSnO₃:Ta thin films with different Ta concentrations

Doping concentration (at.%)	Sn _I 3d5/2	Sn _{II} 3d5/2	Sn _{III} 3d5/2	Sn _I 3d3/2	Sn _{II} 3d3/2	Sn _{III} 3d3/2
0	485.69 eV 14.60 %	486.34 eV 64.04 %	486.97 eV 21.36 %	494.10 eV 14.60 %	494.75 eV 64.04 %	495.38 eV 21.36 %
0.5	485.76 eV 15.30 %	486.43 eV 64.05 %	487.06 eV 20.65 %	494.17 eV 15.30 %	494.84 eV 64.05 %	495.47 eV 20.65 %
1	485.67 eV 19.20 %	486.35 eV 61.73 %	487.01 eV 19.07 %	494.08 eV 19.20 %	494.76 eV 61.73 %	495.42 eV 19.07 %
2	485.79 eV 26.70 %	486.40 eV 56.03 %	487.05 eV 17.27 %	494.20 eV 26.70 %	494.81 eV 56.03 %	495.46 eV 17.27 %
4	485.85 eV 29.49 %	486.47 eV 54.15 %	487.12 eV 16.36 %	494.26 eV 29.49 %	494.88 eV 54.15 %	495.53 eV 16.36 %

As Fig. 7 shows, the carrier concentrations continuously increase with the increase of Ta content. However, the hall mobility decreases generally except 2 at.% doping content, and the resistivity decreases to a minimum value 1.716 Ω cm at 2 at.% tantalum, then begin to increase. According to Eq. 4, the decrease of resistivity is mainly due to the increase of carrier concentration when the doping content is below 2 at.%. The minimum value is a integrated result of increasing carrier concentration and a higher hall mobility at 2 at.% doping content. When the doping content increase to more than 2 at.%, the increase of resistivity is caused by the decrease of hall mobility. As Table 4 shows, the undoped ZnSnO₃ film and Ta doped ZnSnO₃ film have a relatively higher resistivity than some reported ZnSnO₃ films [14, 15, 17], which is assumed to be a result of higher percentage of pores (34 %) in the films by previous SEM analysis. It is noted that the carrier concentration sharply increase from

$8.5 \times 10^{16}/\text{cm}^3$ to $1.152 \times 10^{18}/\text{cm}^3$, thus might be the result of substitution of tantalum in crystal lattice. When the doping content is 2 at.%, the speed-up ratio of carrier concentrations suddenly rise, which is supposed to be related with the different Ta substitution mechanism between Sn⁴⁺ and Zn²⁺ discussed in the previous XPS analysis. As described in Eqs. 2 and 3, the substitution of Zn²⁺ by Ta⁵⁺ generates more electrons than the substitution of Sn⁴⁺, which can increase the carrier concentration significantly. Meanwhile, the increased interstitial Zn²⁺ as shown in XPS also do good to the conductivity [22]. And this substitution mechanism also lead to a sudden increase in Hall mobility at Ta content 2 at.%. Otherwise, in the Ta content regions from 0 to 1 at.% and from 2 to 4 at.%, the decreasing Hall mobility is supposed to be related to the electron scattering effect caused by further increase in Ta doping and grain boundary scattering (Fig. 8).

Fig. 6 XPS spectra for Zn2p of ZnSnO₃:Ta thin films with different Ta concentrations: **a** 0 at.%, **b** 0.5 at.%, **c** 1 at.%, **d** 2 at.% and **e** 4 at.%

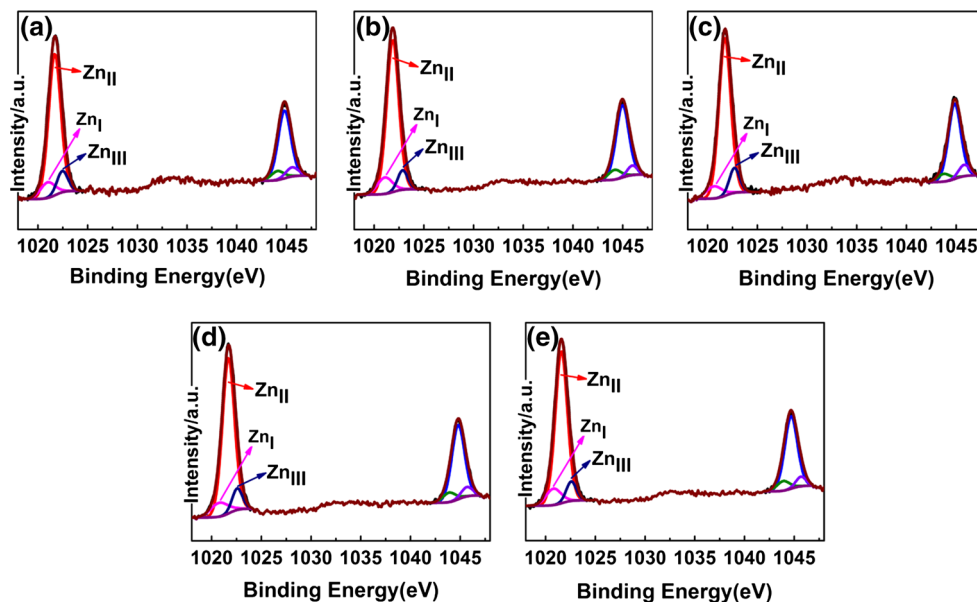


Table 3 XPS peak position of Zn2p in ZnSnO₃:Ta thin films with different Ta concentrations

Doping concentration (at.%)	Zn _I 2p _{3/2}	Zn _{II} 2p _{3/2}	Zn _{III} 2p _{3/2}	Zn _I 2p _{1/2}	Zn _{II} 2p _{1/2}	Zn _{III} 2p _{1/2}
0	1020.92 eV	1021.69 eV	1022.41 eV	1044.02 eV	1044.79 eV	1045.51 eV
	9.36 %	78.74 %	11.90 %	9.36 %	78.74 %	11.90 %
0.5	1020.2 eV	1022.12 eV	1023.04 eV	1044.3 eV	1045.22 eV	1046.14 eV
	8.52 %	79.73 %	11.75 %	8.52 %	79.73 %	11.75 %
1	1020.67 eV	1021.74 eV	1022.7 eV	1043.71 eV	1044.84 eV	1045.8 eV
	8.44 %	80.68 %	10.87 %	8.44 %	80.68 %	10.87 %
2	1020.79 eV	1021.69 eV	1022.58 eV	1043.89 eV	1044.79 eV	1045.68 eV
	10.29 %	80.38 %	9.33 %	10.29 %	80.38 %	9.33 %
4	1020.8 eV	1021.58 eV	1022.83 eV	1043.9 eV	1044.68 eV	1045.68 eV
	10.77 %	80.63 %	8.60 %	10.77 %	80.63 %	8.60 %

Table 4 Carrier concentration, Hall mobility and resistivity of Ta-doped ZnSnO₃ films fabricated with different molar concentrates

Doping concentration (at.%)	Carrier concentration (n, cm ³)	Hall mobility (μ, cm ² /V S)	Resistivity (ρ, Ω cm)
0	8.5 × 10 ¹⁶	1.44	51
0.5	1.152 × 10 ¹⁸	0.544	9.959
1	2.015 × 10 ¹⁸	0.429	7.191
2	6.774 × 10 ¹⁸	0.535	1.716
3	9.033 × 10 ¹⁸	0.191	3.614
4	1.905 × 10 ¹⁹	0.0821	3.982

3.5 Optical properties

UV–Vis spectrum recorded for ZnSnO₃ and Ta-doped ZnSnO₃ films are represented in Fig. 9a. Ta-doped ZnSnO₃ films have better visible transmittance than undoped film

(87.77 %). In addition, the average transmittance is over 91 % in the visible region.

The optical band gaps E_g of the films are calculated from optical transmittance spectrum data by Eq. 5 [40]. In Eq. 5, A is the absorbance, A' is a coefficient, and $h\nu$ is the

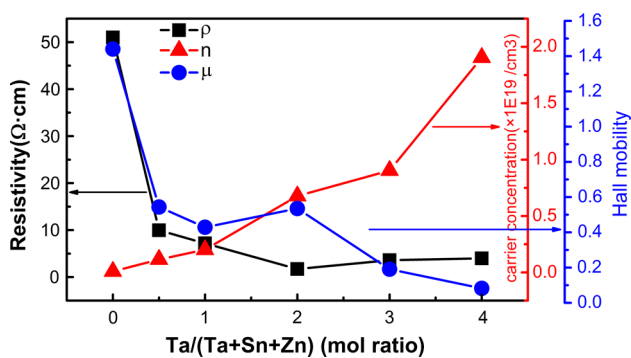


Fig. 7 Electrical properties of the ZnSnO₃:Ta thin films fabricated with different Ta concentration

photon energy. Thus, E_g can be obtained by calculating the $h\nu$ -intercept of a straight-line fitting of $(Ah\nu)^{1/2}$ versus $h\nu$ as shown in Fig. 9b.

$$(Ah\nu)^{1/2} = A'(h\nu - E_g) \tag{5}$$

The E_g value for pure ZnSnO₃ and Ta-doped ZnSnO₃ at different doping level are 3.51 (0 at.%), 3.45 (0.5 at.%), 3.47 (1 at.%), 3.39 (2 at.%) and 3.36 eV (4 at.%), respectively. And the band gap is decreasing with increasing Ta content, which is due to the light doping of Ta. With the doping content increasing, band tailing or impurity band become broader and finally reach and merge the bottom of

the conduction band, which causes the decrease of the optical band gap [41].

3.6 Work function

To obtain work functions of undoped ZnSnO₃ and 2 at.% Ta doped ZnSnO₃, Fermi level E_F was investigated by using electrochemical impedance technique along with Mott-Schottky equation [42, 43], i.e.

$$\frac{1}{C^2} = \frac{2[E - E_F - \frac{kT}{e}]}{\epsilon_0 \epsilon_r N_D} \tag{6}$$

where, C is the capacitance of the space-charge region, ϵ_0 is permittivity of vacuum and ϵ_r is relative permittivity of the sample, N_D is the density of donors, E the applied voltage, κ is Boltzmann’s constant, T is the absolute temperature, and e is the electron charge. Hence, the Fermi level E_F can be obtained from the intercept on the E axis of the linear region of $1/C^2$ against E as shown in Fig. 9. The positive slopes of the linear region of films’ Mott–Schottky curve mean that undoped and Ta-doped ZnSnO₃ are n type semiconductor, which is in agreement with the Hall measurements. The Fermi level E_F of undoped and 2 at.% Ta doped ZnSnO₃ were 0.67 and 0.56 eV (vs. SHE), respectively. The work function of hydrogen is 4.5 eV, thus, the work function of undoped ZnSnO₃ film is 5.17 eV, which is close to the predicted value 5.3 eV [20, 21] and higher

Fig. 8 a Optical transmittance spectra of pure and Ta-doped ZnSnO₃ films; **b** $(Ah\nu)^{1/2}$ versus $h\nu$ plot of pure and Ta-doped ZnSnO₃ films

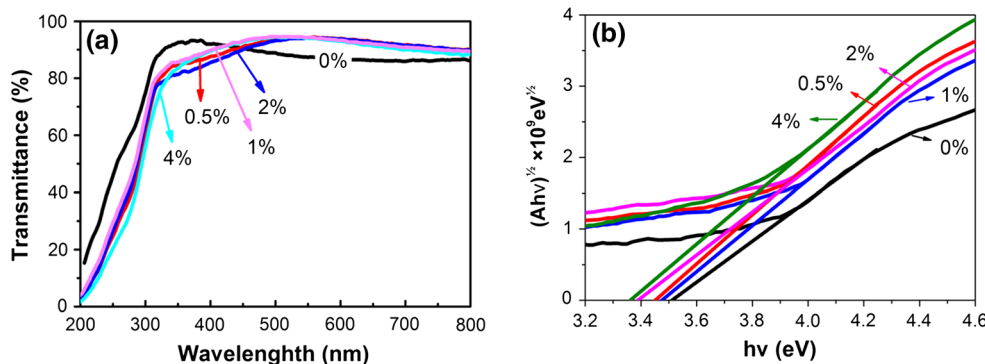
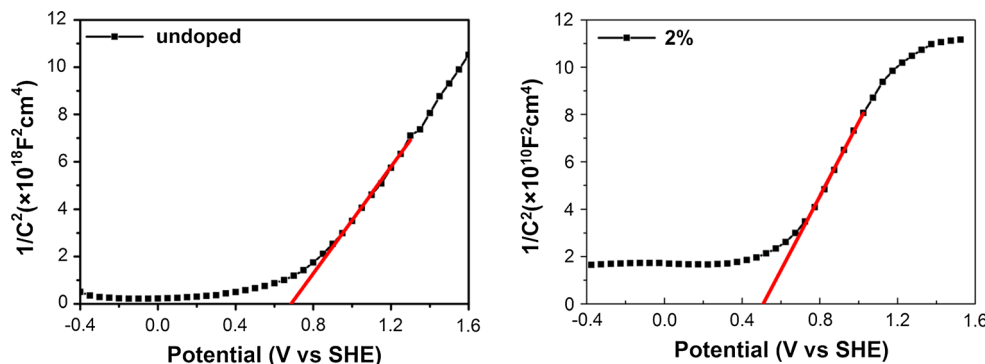


Fig. 9 Mott–Schottky (MS) plots of undoped and 2 at.% Ta doped ZnSnO₃ films



than the reported ITO and FTO(4.4–4.8 eV) [20]. When the doping content increases to 2 at.%, the work function decrease to 5.06 eV. The decrease of work function is assumed to be related to the Fermi level elevation caused by the increasing carrier concentration.

4 Conclusions

In this study, sol–gel spin coating method has been used for the preparation of Ta-doped ZnSnO₃ thin films onto the quartz glass substrates. With the Ta content increasing, there is no other phase but ZnSnO₃, and the crystallinity deterioration is observed in doped films. Tantalum incorporation decreases the grain sizes as well, but has little effects on films' porosity. There might be substitution of Ta⁵⁺ for Sn⁴⁺ when doping content is lower than 2 at.% and substitution of Ta⁵⁺ for Zn²⁺ when doping content is up to 2 at.%, which makes a sudden increase of carrier concentration and abrupt increasing hall mobility. Thus a minimum resistivity of 1.716 Ω cm is obtained for films with 2 at.% Ta. The films' transmittances in the visible range increase up to over 91 % and narrower optical bandgap are observed with increasing Ta concentration. What's more, the work function of ZnSnO₃ is 5.17 eV, and decreased to 5.06 eV when the tantalum concentration is 2 at.%. Both tested work function of Ta doping ZnSnO₃ are higher than ITO, FTO.

References

- D.S. Ginley, C. Bright, *MRS Bull.* **25**, 15 (2000)
- K. Ramamoorthy, M. Jayachandran, K. Sankaranarayanan, P. Misra, L.M. Kukreja, C. Sanjeeviraja, *Sol. Energy* **77**, 193 (2004)
- K. Nomura, H. Ohta, A. Takagi, T. Kamiya, M. Hirano, H. Hosono, *Nature* **432**, 488 (2004)
- W.J. Lee, Y.K. Fang, J.J. Ho, C.Y. Chen, L.H. Chiou, S.J. Wang, F. Dai, T. Hsieh, R.Y. Tsai, D. Huang, F.C. Ho, *Solid State Electron.* **46**, 477 (2002)
- M.G. Helander, Z.B. Wang, J. Qiu, M.T. Greiner, D.P. Puzzo, Z.W. Liu, Z.H. Lu, *Science* **332**, 944 (2011)
- L. Castañeda, *Mater. Sci. Appl.* **02**, 1233 (2011)
- A.J. Freeman, K.R. Poeppelmeier, T.O. Mason, R.P.H. Chang, T.J. Marks, *MRS Bull.* **25**, 45 (2000)
- J.F. Wager, *Science* **300**, 1245 (2003)
- J.H. Ko, I.H. Kim, D. Kim, K.S. Lee, T.S. Lee, J.H. Jeong, B. Cheong, Y.J. Baik, W.M. Kim, *Thin Solid Films* **494**, 42 (2006)
- T.J. Coutts, D.L. Young, X. Li, W.P. Mulligan, X. Wu, *J. Vac. Sci. Technol. A* **18**, 2646 (2000)
- C.-Y. Lo, C.-L. Hsu, Q.-X. Yu, H.-Y. Lee, C.-T. Lee, *J. Appl. Phys.* **92**, 274 (2002)
- J.D. Perkins, J.A. del Cueto, J.L. Alleman, C. Warmsingh, B.M. Keyes, L.M. Gedvilas, P.A. Parilla, B. To, D.W. Readey, D.S. Ginley, *Thin Solid Films* **411**, 152 (2002)
- Y. Hayashi, K. Kondo, K. Murai, T. Moriga, I. Nakabayashi, H. Fukumoto, K. Tominaga, *Vacuum* **74**, 607 (2004)
- V.K. Jain, P. Kumar, M. Kumar, P. Jain, D. Bhandari, Y.K. Vijay, *J. Alloys Compd.* **509**, 3541 (2011)
- M.K. Jayaraj, K.J. Saji, K. Nomura, T. Kamiya, H. Hosono, *J. Vac. Sci. Technol. B* **26**, 495 (2008)
- J.H. Ko, I.H. Kim, D. Kim, K.S. Lee, T.S. Lee, B. Cheong, W.M. Kim, *Appl. Surf. Sci.* **253**, 7398 (2007)
- A. Kurz, M.A. Aegerter, *Thin Solid Films* **516**, 4513 (2008)
- A. Kurz, K. Brakecha, J. Puetz, M.A. Aegerter, *Thin Solid Films* **502**, 212 (2006)
- T. Minami, *MRS Bull.* **25**, 38 (2000)
- T. Minami, T. Miyata, T. Yamamoto, *Surf. Coat. Technol.* **108–109**, 583 (1998)
- M. Tadatsugu, S. Hideo, T. Shinzo, S. Hiroto, Jpn. J. Appl. Phys. **33**, L1693 (1994)
- J. Ling-Li, H. Yun-Qiu, L. Le, *Chin. J. Inorg. Chem.* **28**, 437 (2012)
- G.N. Darriba, E.L. Muñoz, L.A. Errico, M. Rentería, *J. Phys. Chem. C* **118**, 19929 (2014)
- J.-Z. Kong, A.-D. Li, H.-F. Zhai, Y.-P. Gong, H. Li, D. Wu, *J. Solid State Chem.* **182**, 2061 (2009)
- S.W. Lee, Y.-W. Kim, H. Chen, *Appl. Phys. Lett.* **78**, 350 (2001)
- K. Mahmood, D. Song, S.B. Park, *Surf. Coat. Technol.* **206**, 4730 (2012)
- K.S. Kim, W.E. Baitinger, J.W. Amy, N. Winograd, *J. Electron Spectrosc. Relat. Phenom.* **5**, 351 (1974)
- E. Atanassova, D. Spassov, *Appl. Surf. Sci.* **135**, 71 (1998)
- H. Yoon, S. Kim, H. Park, G. Nam, Y. Kim, J.-Y. Leem, M. Kim, B. Kim, Y. Kim, I. Ji, Y. Park, I. Kim, S.-H. Lee, J. Jung, J. Kim, J. Kim, *J. Korean Phys. Soc.* **64**, 109 (2014)
- S.V.J. Chandra, S. Uthanna, G.M. Rao, *Appl. Surf. Sci.* **254**, 1953 (2008)
- X.-L. Li, B.-Z. Lin, B.-H. Xu, Z.-J. Chen, Q.-Q. Wang, J.-D. Kuang, H. Zhu, *J. Mater. Chem.* **20**, 3924 (2010)
- M. Kwoka, L. Ottaviano, M. Passacantando, S. Santucci, G. Czempik, J. Szuber, *Thin Solid Films* **490**, 36 (2005)
- X.-F. Chu, Y.-Q. He, Y.-M. Li, H.-Z. Huang, D.-Y. Liu, H.-M. Chen, W.-Y. Li, *Chin. J. Inorg. Chem.* **5**, 034 (2014)
- J.C.C. Fan, J.B. Goodenough, *J. Appl. Phys.* **48**, 3524 (1977)
- P.K. Biswas, A. De, L.K. Dua, L. Chkoda, *Bull. Mater. Sci.* **29**, 323 (2006)
- Y.-G. Kang, H.-J. Kim, H.-G. Park, B.-Y. Kim, D.-S. Seo, *J. Mater. Chem.* **22**, 15969–15975 (2012)
- K.G. Saw, K. Ibrahim, Y.T. Lim, M.K. Chai, *Thin Solid Films* **515**, 2879 (2007)
- R.W. Mar, *J. Phys. Chem. Solids* **33**, 220 (1972)
- K. Uematsu, N. Mizutani, M. Kato, *J. Mater. Sci.* **22**, 915 (1987)
- A. Ferreira da Silva, N. Veissid, C.Y. An, J. Caetano de Souza, A.V. Batista da Silva, P. César Farias, M.T.F. da Cruz, *J. Appl. Phys.* **78**, 5822 (1995)
- A.A. Dakhel, *Opt. Mater.* **31**, 691 (2009)
- E. Gao, W. Wang, M. Shang, J. Xu, *Phys. Chem. Chem. Phys.* **13**, 2887 (2011)
- K.-P. Wang, H. Teng, *Phys. Chem. Chem. Phys.* **11**, 9489 (2009)